Bioactive Materials 6 (2021) 4415–4429

Contents lists available at ScienceDirect

Bioactive Materials

journal homepage: www.sciencedirect.com/journal/bioactive-materials

Engineering hiPSC-CM and hiPSC-EC laden 3D nanofibrous splenic hydrogel for improving cardiac function through revascularization and remuscularization in infarcted heart

Ge Guan [a], Da Huo [a], Yanzhao Li [a], Xiaolin Zhao [a], Yinghao Li [a], Zhongliang Qin [a,b], Dayu Sun [a], Guanyuan Yang [a], Mingcan Yang [a], Ju Tan [a], Wen Zeng [c,**], Chuhong Zhu [a,*]

[a] Department of Anatomy, State Key Laboratory of Trauma, Burn and Combined Injury, Key Lab for Biomechanics and Tissue Engineering of Chongqing, Army Medical University (Third Military Medical University), Chongqing, 400038, China
[b] Chongqing Institute of Zhong Zhi Yi Gu, Shapingba District, Chongqing, 400030, China
[c] Department of Cell Biology, Third Military Army Medical University, Chongqing, 400038, China

ARTICLE INFO

Keywords:
Stem cell-laden splenic hydrogel
hiPSC differentiation platform
Antioxidant stress
Myocardial infarction
Cardiac repair

ABSTRACT

Cell therapy has been a promising strategy for cardiac repair after myocardial infarction (MI), but a poor ischemic environment and low cell delivery efficiency remain significant challenges. The spleen serves as a hematopoietic stem cell niche and secretes cardioprotective factors after MI, but it is unclear whether it could be used for human pluripotent stem cell (hiPSC) cultivation and provide a proper microenvironment for cell grafts against the ischemic environment. Herein, we developed a splenic extracellular matrix derived thermoresponsive hydrogel (SpGel). Proteomics analysis indicated that SpGel is enriched with proteins known to modulate the Wnt signaling pathway, cell-substrate adhesion, cardiac muscle contraction and oxidation-reduction processes. *In vitro* studies demonstrated that hiPSCs could be efficiently induced into endothelial cells (iECs) and cardiomyocytes (iCMs) with enhanced function on SpGel. The cytoprotective effect of SpGel on iECs/iCMs against oxidative stress damage was also proven. Furthermore, *in vivo* studies revealed that iEC/iCM-laden SpGel improved cardiac function and inhibited cardiac fibrosis of infarcted hearts by improving cell survival, revascularization and remuscularization. In conclusion, we successfully established a novel platform for the efficient generation and delivery of autologous cell grafts, which could be a promising clinical therapeutic strategy for cardiac repair and regeneration after MI.

1. Introduction

Cardiovascular diseases (CVDs) remain the leading cause of global mortality and disease burden according to the Global Burden of Disease (GBD) Study 2019. As reported by the study, the total cases of CVDs nearly doubled from 271 million in 1990 to 523 million in 2019, and the number of CVD deaths increased from 12.1 million in 1990 to 18.6 million in 2019 [1]. Treatment of myocardial infarction (MI) remains a great clinical challenge due to limited myocardial regeneration after MI. Recently, cell therapy based on human induced pluripotent stem cell (hiPSC) derived cardiomyocytes (CMs) [2] or endothelial cells (ECs) [3] has become a promising strategy to obtain a large number of transplanted cells and eliminate immunologic rejection. Several studies have demonstrated that transplantation of hPSC-derived cardiovascular cells promotes cardiac function recovery through the secretion of paracrine factors, reconstitution of extracellular matrix (ECM) and replacement of damaged cardiac tissues, which contribute to the revascularization or remuscularization of infarcted hearts [4]. However, low delivery efficiency and retention of transplanted cells in ischemic heart tissues remain critical barriers for hPSC-derived cell therapy. Active contraction of the heart primarily results in a great loss of transplanted cells [5]. Moreover, the survival rate of transplanted cells is rather poor in the harsh microenvironment, caused by hypoxia, nutrient deprivation, inflammation and oxidative stress [6]. Therefore, the use of

Peer review under responsibility of KeAi Communications Co., Ltd.
* Corresponding author.
** Corresponding author.
E-mail addresses: zengw0105@163.com (W. Zeng), zhuch99@tmmu.edu.cn (C. Zhu).

https://doi.org/10.1016/j.bioactmat.2021.04.010
Received 2 February 2021; Received in revised form 6 April 2021; Accepted 7 April 2021

proper biomaterials combined with cell therapy to provide a suitable microenvironment for implant growth and retention is essential for the study of cardiac regeneration after MI.

Injectable hydrogels have been widely used as cell carriers and scaffolds due to their porous structure and water-swollen polymer networks [7]. Previous studies have reported that injectable hydrogels could be used as effective carriers for delivering therapeutic cells and biomolecules to promote tissue regeneration via a minimally invasive procedure [8,9]. Composed of collagen, elastin, glycosaminoglycans and growth factors, decellularized extracellular matrix (ECM) hydrogels provide transplanted cells with a native cellular microenvironment, and have several advantages over synthetic hydrogels. Recent studies have shown that ECM hydrogels derived from different kinds of ECMs exhibit tissue specificity in tissue regeneration and repair, including stimulating myocardial regeneration (ECM of zebrafish hearts) [10], suppressing oxidative stress (hepatic ECM) [11], and improving the survival and engraftment of transplanted grafts (skeletal ECM) [12].

Recent studies have also shown that newly formed lymphatics in the infarcted heart promote cardiac repair [13,14]. Extracellular proteins secreted by lymphatic ECs were reported to improve neonatal cardiac regeneration and cardiac function after MI [15], suggesting that the ECM proteins of lymphoid organs may play an important role in cardiac repair. The spleen is the largest lymphoid organ in the body. Lieder HR et al. reported that after ischemia/reperfusion, the spleen was activated by vagal nerves to release a cardioprotective factor that could reduce infarct size [16]. Spleen- derived IL-10 was also reported in cardioprotection [17]. Therefore, we investigated whether the splenic extracellular matrix (SpECM) could play a role in improving outcomes after MI. Previous studies have demonstrated that the main components of the decellularized splenic matrix are collagen I, collagen IV, fibronectin, laminin and elastin [18]. It was also reported that cytokines, growth factors and chemokines stored in the SpECM have an impact on the differentiation and commitment of cells in the spleen [19]. *In vitro* experiments suggested that hepatocytes cultured in a decellularized splenic matrix were functionally more active than those cultured under traditional culture conditions [20], and hepatocytes seeded in the spleen were also reported to proliferate and reconfigure *in vivo* [21]. As an adult hematopoietic stem cell niche for extramedullary hematopoiesis [22], the splenic matrix may be used as a platform for stem cell culture and a cell carrier for transplantation.

In this study, we developed an injectable splenic matrix-derived hydrogel (SpGel) that maintains a liquid state at room temperature and is able to solidify and form a nanofibrous scaffold *in vivo* by self-assembly. We hypothesized that the splenic matrix may provide a platform for the culture and differentiation of iPSCs to generate induced endothelial cells (iECs) and cardiomyocytes (iCMs), as well as an efficient carrier for delivering iPSC-derived cardiovascular cells to ischemic mouse hearts. First, hiPSC culture and differentiation on SpGel were studied. Next, SpGel-encapsulated cells were transplanted into ischemic myocardial tissue *in vivo*, and then cell retention, cardiac function, cardiac fibrosis and neovascularization were investigated.

2. Materials and methods

2.1. SpGel preparation and characterization

SpGel Formation: To generate an injectable form of SpGel, porcine spleen tissue was decellularized and solubilized under sterile conditions following a modified protocol reported previously [23,24]. Briefly, the spleen was cut into pieces (approximately 5 mm^3) and washed with phosphate-buffered saline (PBS). Then, the spleen tissue was decellularized by 1% SDS at 25 °C for 48 h and washed with double distilled water for 48 h. Subsequently, the decellularized matrix was frozen (−20 °C) and lyophilized with a freeze dryer (FD-1A-50, BILON, China). After lyophilization, splenic matrix was enzymatically digested with pepsin for 48 h. Next, the pH was adjusted to 7.4 using 1 M NaOH and 10 × PBS. The final concentration of decellularized splenic matrix in the titrated solution was 1.0% (w/v).

2.2. DNA concentration measurement

The residual DNA in SpGel (1.0% w/v) and Matrigel was quantified according to the manufacturer's instructions (DNeasy™, Qiagen, Germany). DNA was extracted from the tissue lysis buffer, and the concentration of DNA in the samples (n = 3) was analyzed on a NanoDrop spectrophotometer (NanoDrop™ 2000/2000c, Thermo Fisher Scientific, America).

2.3. SpGel components quantification

SpGel slides (5 μm) were stained according to the manufacturers' instructions with Picrosirius Red, Verhoeff's and Alcian Blue to assess the retention of collagen, elastin and glycosaminoglycans (GAGs) in SpGel, respectively. Collagen in SpGel was quantified using a QuickZyme Collagen assay kit (QuickZyme Biosciences) [25]. GAG in SpGel was estimated using a GAG quantitation assay kit (GENMED scientifics Inc., USA) via DMMB according to the manufacturer's instructions [26,27].

2.4. Scanning electron microscopy (SEM)

Samples were fixed overnight with glutaraldehyde. Next, the samples were frozen in liquid nitrogen and lyophilized with a freeze dryer. The samples were then mounted onto an aluminum stub and coated with gold particles. SEM images of the samples were analyzed under a scanning electron microscope (CrossBeam 340, Zeiss, Germany) at 10-20 kV.

2.5. Hydrogel rheological measurements

Rheological measurements (n = 3) were taken using a temperature-controlled, 35-mm diameter parallel plate rheometer (HAAKE MARS 60, Thermo, Germany). The samples were added at a temperature of 4 °C, which was then increased to 37 °C to induce gelation. The oscillatory moduli of the samples were monitored at a frequency of 1 Hz and a strain of 1%. After gelation, the samples were subsequently monitored using a frequency sweep under 1% strain, and the storage modulus (G′), loss modulus (G″) and complex viscosity (η*) were measured over a frequency range (0.1–100 rad/s). The viscosity was also measured with a shear rate from 0.001 to 100/s at 37 °C.

2.6. 3D printing of a SpGel patch

The printing process was carried out in a support bath. The fully transparent and biocompatible support bath was prepared as previously described using a microparticulate formulation method [28]. Briefly, 0.1% (w/v) microparticulate (composed of 0.32% (w/v) sodium alginate, 0.25% (w/v) xanthan gum, 9.56×10^{-3} M calcium carbonate and 19.15×10^{-3} M D-(+)-gluconic acid δ-lacton) was resuspended in 1% (w/v) xanthan gum to form the support bath. The bioink at a 3% (w/v) concentration was generated by dissolving lyophilized SpGel powder in PBS solution, which was supplemented with 0.04% (v/v) blue food dye to visualize the printing process and the final pattern. A 10-ml syringe fitted with a 30G needle was loaded with freshly prepared bioink (5 ml) and then mounted onto a 3D extrusion printer (3D-bioplotter, Envisiontec). The extrusion pressure and printing speed were kept constant at 1 bar and 25 mm/s, respectively. After printing, the SpGel hydrogel in the support bath solidified at 37 °C to form the designed pattern.

2.7. Label-free quantitative proteomics

Label-free quantitative proteomics was used to analyze the retained

protein content of pepsin-digested SpECM (Sp-Gel) and myocardial ECM (Myo-Gel) [24]. Protein of lyophilized Sp-Gel and Myo-Gel was extracted by SDT lysis buffer (4% SDS, 100 mM DTT, 100 mM Tris-HCl pH 8.0), and the protein concentration was determined by a BCA Protein Assay Kit (Thermo Fisher Scientific). Protein tryptic digestion was processed by filter-aided sample preparation (FASP). The peptide was desalted with C18 StageTip for further LC-MS analysis. One hundred micrograms of extracted peptide samples was lyophilized and fractionated in a reverse-phase column at a high pH in preparation for liquid chromatography-tandem mass spectrometry (LC-MS/MS). Chromatographic separations were performed on an Easy nLC 1200 chromatography system. Quantitative analysis of the samples was carried out on a Q-Exactive Plus mass spectrometer (Thermo Scientific) using data-dependent acquisition (DDA). MS data were acquired using a data-dependent top20 method by dynamically choosing the most abundant precursor ions from the survey scan (300–1800 m/z) for high-energy collision dissociation (HCD) fragmentation. The MS data were analyzed using MaxQuant software version 1.6.0.16. The MS data were searched against the UniProt Protein Database (50331 total entries, downloaded 04/02/2019). Label-free quantification was carried out in MaxQuant.

2.8. Differentiation of hiPSCs into ECs and CMs

hiPSCs were provided by the National Collection of Authenticated Cell Cultures (DYR0100, NCACC). The undifferentiated cells were cultured on SpGel-coated plates, which were maintained in mTeSR™1 medium (StemCell Technologies, Canada) at 37 °C with 5% CO_2. The medium was refreshed daily.

EC Differentiation of iPSCs: Cells were differentiated as previously described with modifications [29]. Briefly, differentiation was initiated after the cells reached 60% confluency. On day 0, the medium was changed to RPMI-1640 containing 2% B-27 minus insulin (both from Gibco) and 5 μM CHIR99021 (Selleckchem). On day 2, the medium was changed to RPMI-1640 containing 2% B-27 minus insulin (both from Gibco) and 2 μM CHIR99021 (Selleckchem). From day 4 to day 7, the cells were exposed to RPMI-1640 containing 2% B-27 minus insulin plus 50 ng/ml vascular endothelial growth factor (VEGF; R&D Systems), 10 ng/ml fibroblast growth factor basic (FGFb; R&D Systems), 10 μM Y-27632 (Sigma-Aldrich) and 1 μM SB 431542 (Sigma-Aldrich). From day 7, the cells were maintained in EGM-2 (Lonza) plus 10% HI-FCS (Gibco), 25 ng/ml VEGF, 2 ng/ml FGFb, 10 μM Y-27632 (Sigma-Aldrich) and 1 μM SB 431542. EC differentiation was achieved after 14 days. The induced cells were treated with 20 μM PluriSln-1 (StemCell Technologies) for 48 h to obtain purified EC clusters.

CM Differentiation of iPSCs: Cells were differentiated as previously described [30]. Briefly, after iPSCs reached 85% confluence (day 0), the medium was changed to RPMI-1640 medium (11875, Life Technologies), 213 μg/ml L-ascorbic acid 2-phosphate (Sigma-Aldrich), 500 μg/ml *O. sativa*–derived recombinant human albumin (A0237, Sigma-Aldrich) and 6 μM CHIR99021 (Selleckchem). On day 2, CHIR99021 was removed from the media, and 2 μM Wnt-C59 (Selleck Chemicals) was added. At day 4, Wnt-C59 was removed. The medium was changed every other day (48 h), and contracting cells were observed from day 7. The contractile frequency was observed by a Leica microscope and recorded with a video camera.

2.9. Flow cytometry analysis

Staining of the surface markers APC-CD31 (BioLegend), PerCP/Cy5.5-CD144 (BioLegend) and mouse IgG2a (BioLegend) was performed in PBS containing 2% fetal bovine serum (v/v) on ice. Flow cytometry data were obtained with a FACSCanto II (BD Biosciences) and analyzed by using FlowJo software (Tree Star).

2.10. Vascular tube formation

hiPSC-derived ECs induced on SpGel were grown in EGM-2 media. iECs were transferred to 24-well plates precoated with Matrigel at a density of 120,000 cells in 300 μl media per well. Approximately 8 h after plating, the cells were incubated with calcein AM following the manufacturer's instructions (BestBio) and imaged for endothelial tube formation under green fluorescent light (Evos FL Auto, Life Technologies).

2.11. Beating rate analysis and field potential recordings of hiPSC-derived CMs

Beating rates of hiPSC-derived iCMs induced on SpGel or Matrigel were recorded on a Leica microscope. The field potential was recorded using a multielectrode array (MEA) system. The iCMs induced on SpGel or Matrigel were transferred to a Matrigel-precoated (1:100 dilution) 24-well MEA plate (5×10^4 cells per well) (AXION, Atlanta, GA, USA). Field potentials were recorded 1 week after seeding using Axion BioSystems' Maestro MEA systems. Field potential signals were analyzed with the Axion Cardiac Data Plotting Tool.

2.12. Cytoprotection of iECs/iCMs against oxidative stress by SpGel encapsulation

To investigate the cytoprotective effects of encapsulation with SpGel on iECs/iCMs against oxidative stress, SpGel-encapsulated iECs/iCMs and nonencapsulated iECs/iCMs were cultured in normal EGM-2 medium or an ROS microenvironment containing 200 μM H_2O_2. After exposure to H_2O_2 for 2 h, Live/Dead staining was performed on the cells following the manufacturer's instructions (BestBio).

2.13. Transmission electron microscopy

After exposure to H_2O_2 for 2 h, SpGel-encapsulated iECs/iCMs and iECs/iCMs alone were harvested, fixed with 1% glutaraldehyde in PBS for 12 h and washed with PBS. Next, the samples were fixed with 1% osmium tetroxide in PBS for 1 h. Then, the samples were dehydrated using an ethanol series from 50% to 100%. After that, the samples were impregnated with epoxy resin and polymerized in plastic dishes at 40 °C for 48 h. Uranyl acetate and lead citrate staining were performed after sectioning. Imaging was performed using a Hitachi H-7000 transmission electron microscope (Hitachi).

2.14. Animal care and surgical procedure

All animal experiments were approved by the Ethics Committee of the Army Medical University, China. Experiments were carried out in accordance with the regulations of ethical approval for research on laboratory animals. Male C57BL/6J mice (8–12 weeks) were purchased from the Laboratory Animal Center of the Army Medical University. Mouse MI was performed as described previously. In brief, mice were anaesthetized with 1.0% inhaled isoflurane, and breathing was maintained by a ventilator. The left anterior descending (LAD) coronary artery was ligated with an 8-0 nylon suture after exposing the heart. These MI models were randomly divided into 5 groups as follows ($n = 6$ in each group): (1) Sham, (2) PBS, (3) iECs/iCMs alone, (4) SpGel alone, and (5) iECs/iCMs + SpGel. A total of 1×10^5 iECs and 2×10^5 iCMs were resuspended in 20 μl SpGel or PBS and intramyocardially injected into the border region of the infarct area with 30G needles at 3 sites of the myocardium. Mice were treated with cyclosporin A (10 mg/kg/day, Neocyspin) every day until the end of the study.

2.15. Survival analysis of cell grafts using IVIS

MI was performed as described previously. To track the cell grafts *in*

vivo, iECs/iCMs (3×10^5; iCMs and iECs at a ratio of 2:1) were incubated with DiR (AAT Bioquest, USA) according to the manufacturer's instructions. MI model mice were randomly divided into 2 groups as follows (n = 4 in each group): (1) DiR-iECs/iCMs and (2) DiR-iECs/iCMs encapsulated in SpGel. A total of 1×10^5 iECs and 2×10^5 iCMs were resuspended in 20 μl SpGel or PBS and intramyocardially injected into the hearts. On days 0 and 7, the mice were imaged under general anesthesia with 1.0% inhaled isoflurane using the IVIS 200 system (Xenogen). The maximum signal from an ROI was measured using Living Image software (Media Cybernetics).

2.16. Histology analysis of cell retention in the mouse hearts

To investigate the effects of SpGel on cell engraftment *in vivo*, iECs/iCMs were prelabeled with PKH26 (Sigma-Aldrich) following the manufacturer's instructions and injected into the hearts (n = 6 per group). On days 1 and 7, MI mice were euthanized, and their hearts were rapidly excised. After fixation in 4% paraformaldehyde and dehydration in 30% sucrose solution, the samples were embedded in OCT and cut into sections (7 μm). Hematoxylin and eosin (H&E) staining was performed, and the samples were imaged with a Leica microscope. The nuclei were stained with DAPI (Invitrogen). The immunofluorescence-stained sections were imaged with a fluorescence microscope (Evos FL Auto, Life Technologies).

2.17. Echocardiographic measurement

On day 28 after surgery, the mice were anaesthetized with 1.0% inhaled isoflurane, and echocardiography was performed on a Vevo 2100 (Visual Sonics, Canada). Left ventricular ejection fraction (LVEF), fractional shortening (LVFS), left ventricular systolic diameter (LVSD) and left ventricular diastolic diameter (LVDD) were calculated using two-dimensional and M-mode images.

2.18. H&E and masson staining

At day 28 after the surgery, mice were euthanized, and the hearts were excised. After washing with PBS, the hearts were fixed in 4% paraformaldehyde, embedded in paraffin and cut into sections (4 μm). Masson's trichrome and H&E staining were performed to analyze the infarct size of the infarct zone.

2.19. Immunostaining

Heart sections were stained with anti-MLC2V (Proteintech; 1:50), anti-α-SMA (BOSTER; 1:50) and anti-CD31 (Abcam, 1:50) at 4 °C overnight. The samples were washed with PBS and then incubated with secondary antibodies at room temperature for 1 h. DAPI was used for nuclear staining. The immunofluorescence-stained sections were imaged with a Zeiss confocal microscope.

2.20. Statistical analysis

Statistical analyses were performed using GraphPad Prism 6.0 software with significance defined as $p < 0.05$. The results are reported as the mean ± standard deviation (SD). One-way analysis of variance (ANOVA) was performed for analysis of variance between more than two groups. Student's t-test was used for comparisons between two groups.

3. Results

3.1. Formation and characterization of thermoresponsive SpGel

SpGel was derived from decellularized porcine spleen tissue, which was enzymatically dissolved to obtain a liquid thermoresponsive hydrogel (Fig. 1A). The liquid SpGel gelated after it was heated to 37 °C *in vitro* or injected *in vivo*. H&E and Masson staining demonstrated that cellular debris was removed after decellularization (Fig. 1B and C). The collagen and glycosaminoglycan (GAG) contents were also quantified (436.97 ± 28.92 μg/mg and 4.19 ± 0.71 μg/mg, respectively, Fig. 1D). Histological analysis confirmed the retention of collagens, elastin and GAG in SpGel (Fig. 1E). SEM analysis demonstrated the porous nanofibrous structure of SpGel with an average fiber diameter of 66.67 ± 10.60 nm, while Matrigel exhibited a porous structure (20.16 ± 7.04 μm) without nanofibers (Fig. 1F). Quantitative analysis of DNA content confirmed a large reduction in DNA after decellularization (49.10 ± 13.90 ng/ml), which was much lower than Matrigel (126.70 ± 5.92 ng/ml, Fig. 1G). A previous study reported that nanofibrous scaffolds possess more biomimicking properties since the majority of ECM proteins are fibrous [31]. To evaluate the viscoelastic properties of SpGel, the storage and loss modulus (G′ and G″) of SpGel were determined with a rheometer, showing the gelation process by rapidly increasing the temperature from 4 °C to 37 °C (Fig. 1H, i). The loss modulus (G″) was greater than the storage modulus (G′) before gelation, while the storage modulus (G′) was 10-fold greater than the loss modulus (G″) after gelation. The gelation time (time to 50% gelation) of SpGel was 1–2 min. After gelation at 37 °C, the storage modulus (G′), loss modulus (G″) and complex viscosity (η*) were measured over a frequency range of 0.1–100 rad/s (Fig. 1H, ii). The viscosity of SpGel decreased with an increase in shear rate, which indicated that SpGel exhibited shear-thinning behavior (Fig. S1). Due to the high thermoresponsive property of SpGel, we further investigated its potential for direct 3D bioprinting of tissue scaffolds in a fully transparent supporting medium. SpGel labeled with blue food dye was used as a bioink for the direct printing of reticulate patches (Fig. 1I, i). After printing, the printed reticulate patch gelated in the supporting medium under the control of temperature-driven gelation (Fig. 1I, ii and iii). To assess the cytocompatibility of SpGel as a cell scaffold, a CCK-8 assay was carried out, which showed no significant difference between the SpGel group and the control group (Fig. S2). The biodegradability of SpGel was also analyzed by subcutaneous implantation, and the percentage of SpGel remaining significantly decreased (30.85 ± 9.69%) on day 14, implying that SpGel is degradable (Fig. S3).

3.2. Tissue-specific ECM components between the Sp-Gel and Myo-Gel

To identify tissue-specific protein components in the pepsin-digested SpECM (Sp-Gel) and mECM (Myo-Gel), label-free MS-based proteomics analysis was conducted. SDS-PAGE analysis showed that Sp-Gel shared multiple components with Myo-Gel, and spleen-specific protein components were further validated (Fig. 2A). The proteomic analysis demonstrated that 1481 and 1065 protein species were identified in Sp-Gel and Myo-Gel, respectively. Sp-Gel and Myo-Gel shared 858 protein species, approximately 80% of the total protein species in Myo-Gel (Fig. 2B). Hierarchical clustering analysis identified differentially expressed proteins between the two groups (Fig. 2C). Subsequently, Gene Ontology (GO) and Kyoto Encyclopedia of Genes and Genomes (KEGG) enrichment analyses were conducted. In Fig. 2D and E, different function-related proteins were divided into two groups, namely, the splenic-specific protein group (spleen specific) and the group of proteins expressed in both Sp-Gel and Myo-Gel but with higher expression in Sp-Gel (both). Proteins related to the biological processes of extracellular structure organization, small molecule metabolic process, extracellular structure organization, cell-substrate adhesion, cell junction organization, and cell migration were more highly expressed in Sp-Gel than in Myo-Gel. The molecular functions extracellular exosome, adherens junction and cell adhesion molecule binding proteins were differentially expressed between the two types of tissues. In addition, GO enrichment analysis revealed downregulated oxidation-reduction process-related proteins in Sp-Gel (Fig. S4). Differentially expressed proteins associated with apoptosis, gap junctions, tight junctions, adherens junctions, focal

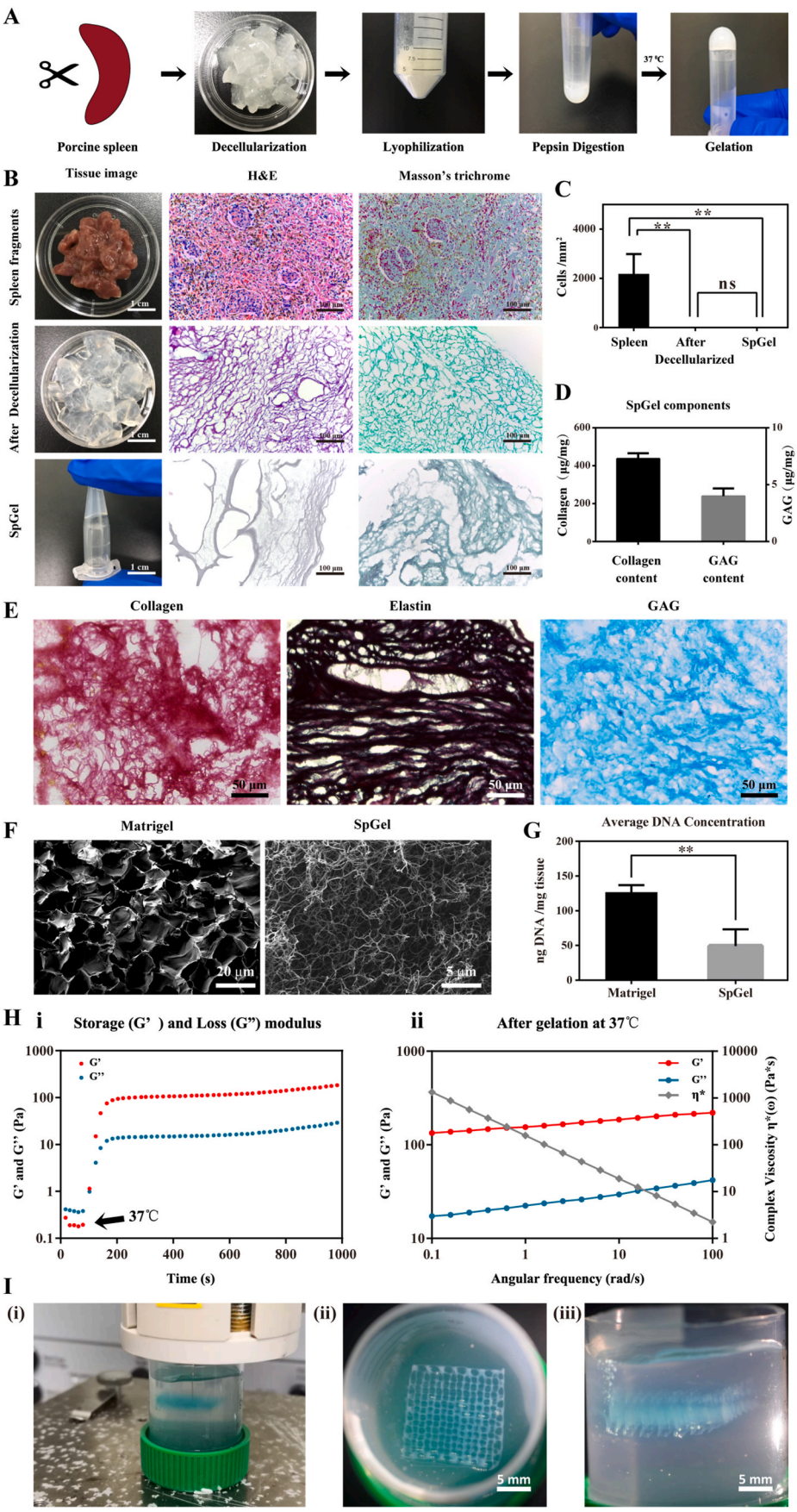

Fig. 1. Characterization of the splenic ECM-based nanofibrous hydrogel. (A) Schematic showing the preparation of the splenic ECM-based hydrogel. (B) Splenic tissue decellularization confirmation with macroscopic and microscopic appearance. (C) Comparison of cell density measured by H&E and Masson staining (** $p < 0.01$). (D) Quantitative analysis of collagens and GAGs in SpGel. (E) Histological sections of SpGel stained with Picrosirius Red, Verhoeff's and and Alcian Blue for collagen, elastin and glycosaminoglycans, respectively. (F) Scanning electron microscopy (SEM) images of Matrigel and SpGel. (G) DNA quantification of SpGel and Matrigel (n = 3, ** $p < 0.01$). (H) Rheological measurements of SpGel. (i) Representative curves of the storage (G'; red) and loss modulus (G"; blue), showing gelation kinetics at 37 °C. (ii) Representative graph of the storage modulus (G'; red), loss modulus (G"; blue), and complex viscosity (η*; gray) of SpGel after gelation at 37 °C, plotted over angular frequency. (I) 3D printing of the SpGel bioink in a supporting medium. (i) SpGel patches were printed in a supporting medium through an extrusion-based 3D bioprinter (0.04% (v/v) blue food dye was added to the SpGel bioink). (ii) Top and (iii) side views of a 3D-bioprinted multilayered mesh pattern (15 × 15 × 2 mm). (For interpretation of the references to color in this figure legend, the reader is referred to the Web version of this article.)

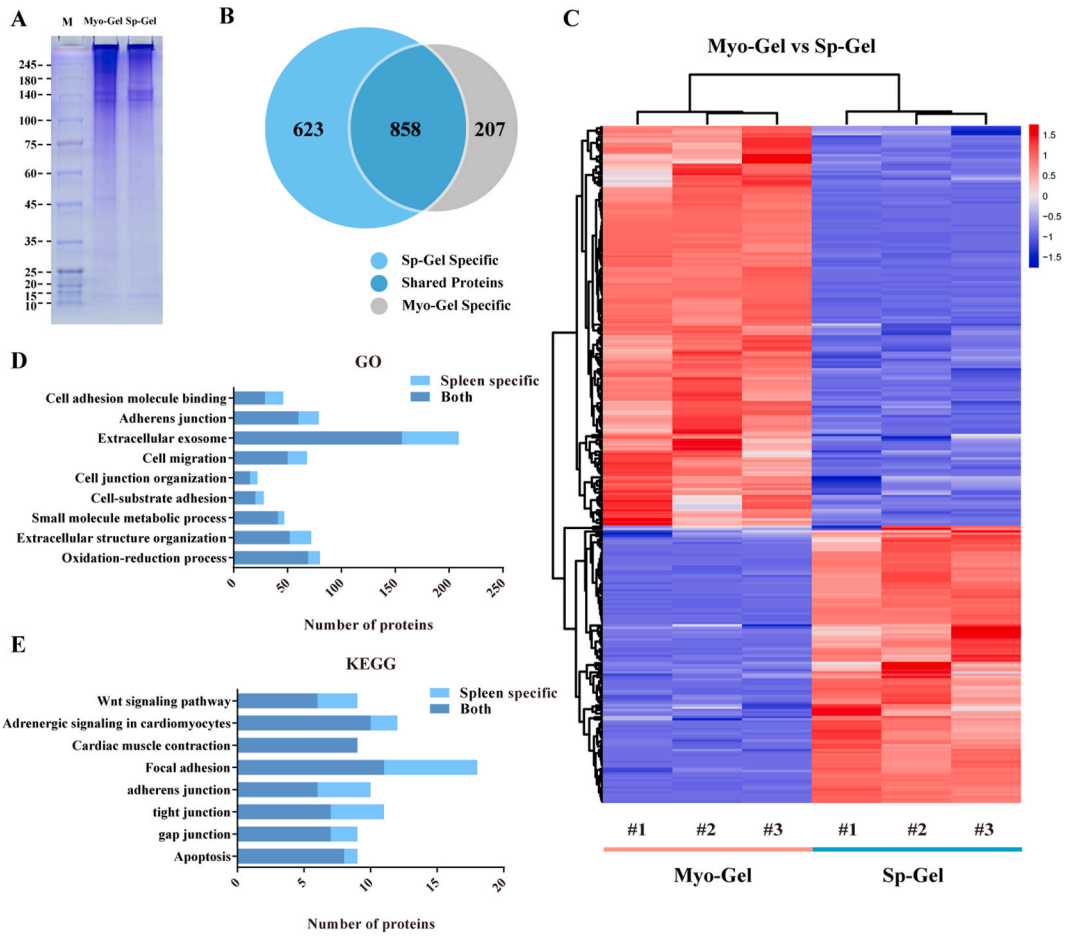

Fig. 2. Proteomic analysis and validation. (A) SDS-PAGE gel analysis of Sp-Gel and Myo-Gel. (B) Venn diagram showing the proteomic results of Sp-Gel and Myo-Gel. (C) Heatmap of cluster analysis of proteins within the Myo-Gel and Sp-Gel, n = 3. (D) Gene Ontology (GO) term enrichment analysis and (E) Kyoto Encyclopedia of Genes and Genomes (KEGG) enrichment analysis of proteins within Sp-Gel and Myo-Gel. Comparison between spleen-specific proteins (spleen specific) and more highly expressed proteins in Sp-Gel (both).

adhesion, cardiac muscle contraction, adrenergic signaling in CMs and the Wnt signaling pathway are shown in Fig. 2E.

3.3. SpGel provided a platform for hiPSC differentiation

ECM viscoelasticity has been reported to affect cell growth, proliferation, migration and differentiation by cell–matrix interactions via mechanosensitive molecular pathways [32]. To explore the pluripotency of hiPSCs after seeding on SpGel-covered dishes, the expression of the pluripotent marker protein OCT4 was confirmed by immunostaining (Fig. 3B). Next, hiPSCs were exposed to an endothelial differentiation protocol [29], as shown in Fig. 3A. Immunofluorescence analysis demonstrated that iECs highly expressed the endothelial markers vWF and CD31 (Fig. 3B). FACS analysis revealed that the proportion of CD31+/CD144+ cells increased from 0.05% to 94.6% after differentiation (Fig. 3C). SEM revealed the morphology of iECs on the nanofibrous SpGel (Fig. 3D). Filopodia and protein filaments were observed on the surface of spreading iECs, suggesting the adhesion and survival of iECs on SpGel, as well as cell-matrix interactions. Next, we compared the tube formation capacity of iECs with that of HUVECs (Fig. 3E). Tube length was slightly higher in the iEC group than in the HUVEC group, and there was no significant difference in the number of branches between the two groups. The results confirmed the functional characteristics of ECs induced on SpGel. qPCR also confirmed that iECs highly expressed CD31, CD144, vWF and CDH5 (Fig. S5, i). Furthermore, SpGel was mixed with calcein-AM-labeled iECs for 48 h. The reconstructed 3D movie shows the 3D growth and tube formation ability of iECs on SpGel at different photographed focal planes (Movie S1).

Supplementary data related to this article can be found at https://doi.org/10.1016/j.bioactmat.2021.04.010.

Cardiomyocyte differentiation [30] was also induced on SpGel following a cardiac lineage differentiation protocol (Fig. 4A). Immunofluorescence staining demonstrated that iCMs highly expressed cardiomyocyte-specific marker proteins, such as α-actinin, cTnT and MLC2V (Fig. 4B). qPCR also confirmed that iCMs expressed MYL3, SLC8A1 and TNNT2 (Figure S5, ii). The morphology of iCMs on SpGel was shown by SEM (Fig. 4C). The results demonstrated that the myocardial fiber bundles were arranged tightly and regularly. To explore the function of iCMs, contractile frequency was recorded with a video camera (Movies S2 and S3), iCMs induced on SpGel revealed an increased contraction amplitude and a higher beating frequency (approximately 60 beats/min) than iCMs induced on Matrigel-covered dishes (approximately 10 beats/min). To explore the electrophysiological features of iCMs induced on SpGel or Matrigel-covered dishes, a multielectrode array (MEA) system was used to record the field potential in real time. MEA analyses revealed that iCMs induced on SpGel showed a higher beating frequency of approximately 63.38 ± 2.76 beats/min compared to the iCMs induced on Matrigel-covered dish (13.92 ± 3.50 beats/min), and a higher field potential (FP) amplitude was observed (Fig. 4E). The field potential duration (FPD) of iCMs induced on SpGel (391.43 ± 43.71 ms) was significantly increased compared with those induced on Matrigel-covered dishes (104.62 ± 23.17 ms), which indicated that iCMs induced on SpGel may promote functional improvement during CM differentiation (Fig. 4D). Furthermore, the ultrastructure of

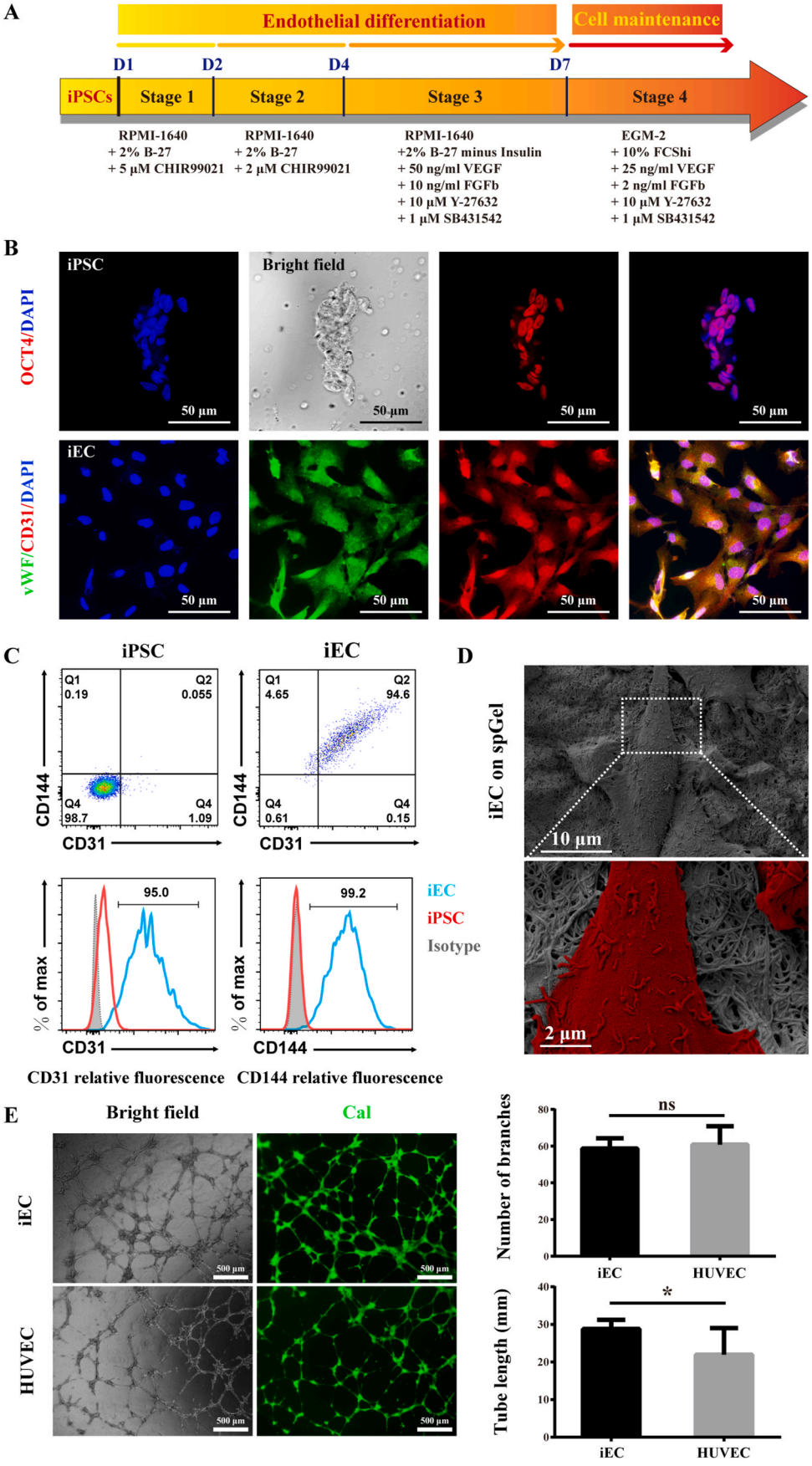

Fig. 3. Differentiation of hiPSCs into induced endothelial cells (iECs) on SpGel. (A) Schematic of the hiPSC-EC differentiation protocol. (B) Immunostaining of undifferentiated hiPSCs and iECs. hiPSCs were confirmed via the expression of OCT4 (red), while iECs were confirmed via the concomitant expression of vWF (green) and CD31 (red). (C) The differentiation of the iEC population was evaluated by flow cytometry analysis of CD31 and CD144 coexpression. Flow cytometry analysis of CD31 and CD144 expression in iPSCs and iECs. (D) Pseudocolor SEM images of hiPSC-ECs (red) on SpGel. (E) hiPSC-ECs and HUVECs formed tubular structures and were stained for calcein AM (green). Quantitative analysis of vascular tube formation shows the number of branches and the tube length (* $p < 0.05$). (For interpretation of the references to color in this figure legend, the reader is referred to the Web version of this article.)

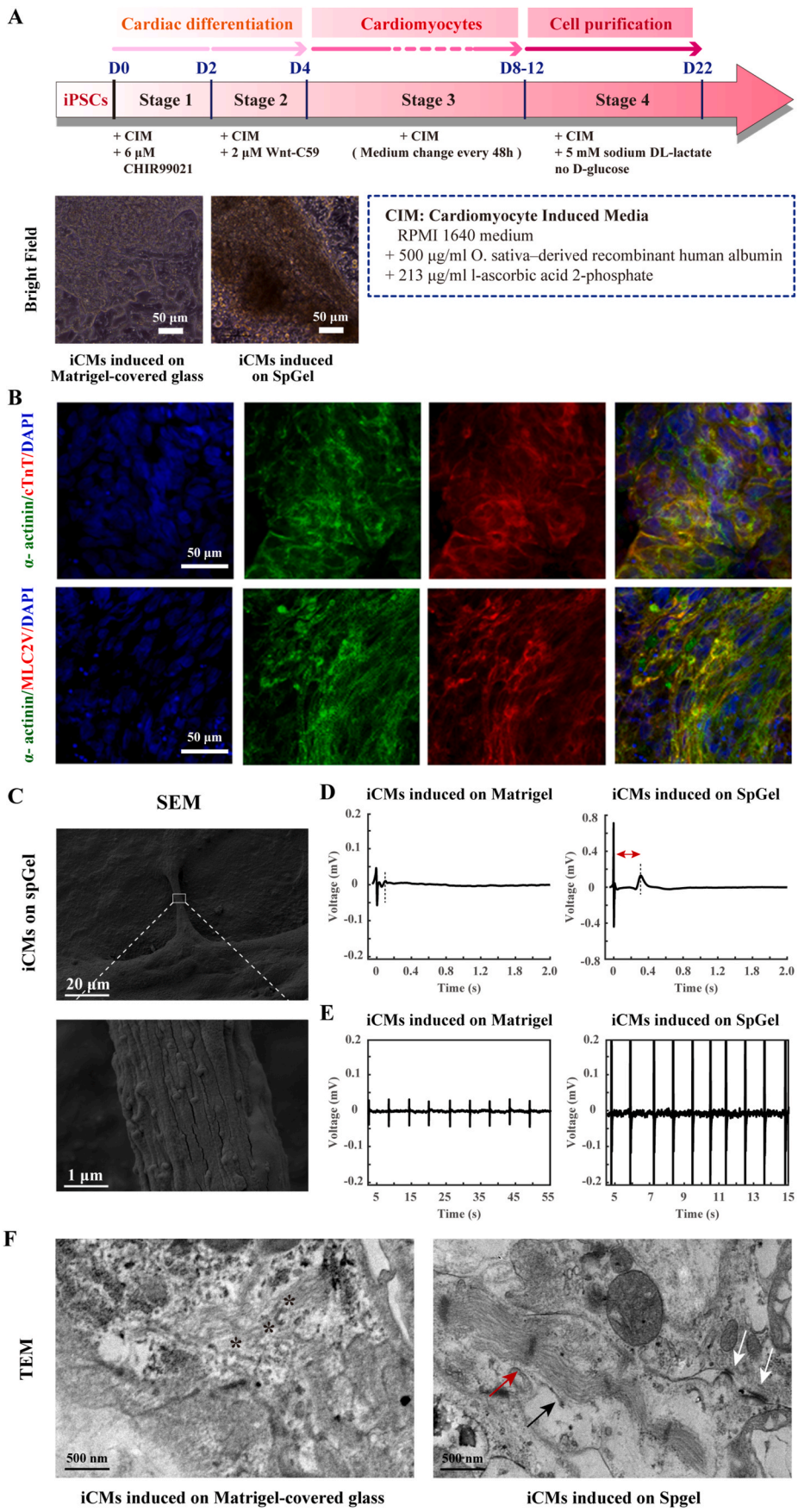

Fig. 4. Differentiation of hiPSCs into induced cardiomyocytes (iCMs) on SpGel. (A) Schematic of the hiPSC-CM differentiation protocol. Bright-field images of iCMs induced on Matrigel- or SpGel-covered dishes. (B) Immunostaining of hiPSC-derived CMs (iCM) for α-actinin (green), cTnT (red), MLC2V (red) and nuclei (blue). (C) SEM images of hiPSC-CMs on SpGel. (D) Representative traces of averaged field potential (FP) of iCMs induced on SpGel- or Matrigel-covered plates recorded by MEA (n = 16). (E) Representative raw traces of MEA recordings from different groups of hiPSC-derived CMs. (F) Ultrastructural analysis of iCMs generated on SpGel- or Matrigel-covered glass by transmission electron microscopy (TEM) to identify myofibrils (Mf), Z-lines and gap junctions. Representative areas of sarcomeric disarray are indicated (*). Sarcomeres, Z-line structures and gap junctions are indicated by black arrows, red arrows and white arrows, respectively. (For interpretation of the references to color in this figure legend, the reader is referred to the Web version of this article.)

iCMs (Fig. 4F) generated on SpGel- or Matrigel-covered glass was characterized by transmission electron microscopy (TEM). Sarcomeres, Z-line structures and gap junctions were clearly observed in the SpGel group, while in the Matrigel-covered glass group, sarcomeric disarray without Z-line structures was observed. These results indicated that SpGel could interact with seeded cells and promote the structural maturation of iCMs.

Supplementary data related to this article can be found at https://doi.org/10.1016/j.bioactmat.2021.04.010.

3.4. Cytoprotective effect of SpGel on oxidant stress damage in iECs/iCMs

Since hypoxia and oxidative stress are suggested to be the main causes of the death of transplanted cells in the ischemic area [33], we next examined whether the encapsulation of iECs/iCMs with SpGel could protect the cells from oxidative stress *in vitro*. As shown in Fig. 5A, iPSC-derived ECs and iPSC-derived CMs were harvested from SpGel-covered plates and encapsulated within the nanofibrous SpGel for 3D culture. Pseudocolor SEM and H&E staining images revealed the morphology and distribution of iECs/iCMs within SpGel. The co-cultured iECs and iCMs were characterized by immunofluorescence staining 48 h after coculture (Fig. 5B). Confocal microscopic examination demonstrated cell membrane interactions between iECs (red, huCD31) and iCMs (green, α-actinin). Next, 200 μM H_2O_2 was added to induce oxidative stress damage. The cytoprotective effects of SpGel on the survival of iECs/iCMs were explored by live/dead staining (Fig. 5C) following 2 h of H_2O_2 treatment. No significant difference was found between the SpGel and control groups before H_2O_2 treatment (Fig. 5D), which indicated that SpGel supported cell growth without cytotoxicity ($p = 0.9975$). Compared with the normal control, H_2O_2 induced massive cell death ($p < 0.0001$), and viability was significantly improved in the presence of SpGel compared with the absence of SpGel ($p < 0.0001$). TEM graphs (Fig. 5E) demonstrated disrupted cytoarchitecture, cell vacuolation and necrosis in cells without SpGel after treatment with H_2O_2. However, cells on SpGel appeared to be free of serious structural deformity, and autophagic vacuoles in the cytoplasm were observed. These results indicated that encapsulation of iECs/iCMs within SpGel could protect cultured cells from oxidative stress damage.

3.5. Survival of cell grafts after transplantation into mouse MI hearts

A schematic of the animal experiment is presented in Fig. 6A. The MI mouse model was created by ligation of the left anterior descending artery. To investigate the effects of SpGel on iEC/iCM engraftment and survival *in vivo*, we prelabeled iECs/iCMs with DiR and injected them into infarcted mouse hearts with or without SpGel. Seven days after injection, fluorescent imaging revealed that SpGel encapsulation significantly improved cell retention in the ischemic heart (Fig. 6B and E, $p = 0.0014$). To confirm iEC/iCM retention, hearts were excised and placed in an IVIS Imaging System to track DiR-iEC/iCM immunofluorescence on day 3 post injection (Fig. 6C). A quantitative analysis revealed that the fluorescence intensity of the cells-SpGel group was 6 times higher than that of the cell-only group (Fig. 6F, $p = 0.0260$). Subsequently, PKH26-labeled SpGel-iECs/iCMs and PBS-iECs/iCMs were injected into the infarcted hearts. H&E staining and immunostaining (Fig. 6D and G) analyses of sectioned heart tissues indicated that the retention rate of SpGel-iECs/iCMs was approximately 7-fold and 3-fold higher than that of PBS-iECs/iCMs on day 1 ($p < 0.0001$) and day 7 ($p = 0.0376$), respectively. These results suggested that encapsulation in SpGel significantly increased the retention of the cell grafts in the mouse hearts.

3.6. In vivo evaluation of cardiac function, cardiac fibrosis and angiogenesis

We further investigated the therapeutic effects of iECs/iCMs encapsulated with SpGel on MI mice. After MI induction, mice were randomized into five groups: (1) sham, thoracotomy without MI surgery; (2) MI + PBS alone, intramyocardially injected with 20 μl of PBS; (3) MI + SpGel alone, intramyocardially injected with 20 μl of SpGel; (4) MI + iECs/iCMs in PBS, intramyocardially injected with 3×10^5 iECs/iCMs in 20 μl of PBS; and (5) MI + iECs/iCMs in SpGel, intramyocardially injected with 3×10^5 iECs/iCMs in 20 μl of SpGel. To evaluate the therapeutic effects of grafts on cardiac function in MI mice, echocardiography was performed 4 weeks post injection. As shown in Fig. 7A, the SpGel-iEC/iCM group had significantly increased left ventricular ejection fraction (LVEF) and decreased left ventricular systolic diameter (LVSD) and LV diastolic diameter (LVDD) compared to the PBS group. The PBS group (31.68 ± 2.17%) showed a 33.67 ± 1.69% decrease in LVEF compared to the sham group (65.35 ± 5.39%). Injection of SpGel-iECs/iCMs led to the highest LVEF measurements (54.53 ± 2.09%) at 4 weeks, while the PBS-iEC/iCM group (46.88 ± 1.73%) and SpGel group (39.91 ± 1.34%) showed a slight increase in LVEF compared to the PBS group (Fig. 7B). Representative videos of cardiac ultrasound are shown in the supplemental material (Movies S4-8). The results revealed that treatment with SpGel-iECs/iCMs promoted a higher recovery of cardiac function than any other treatment. Furthermore, Masson staining at 4 weeks revealed that infarct fibrosis was reduced by injection of iECs/iCMs encapsulated with SpGel (Fig. 7C). As shown in Fig. 7C and D, treatment of MI with SpGel-iECs/iCMs (16.64 ± 4.59%) significantly decreased the extent of infarct fibrosis compared to treatment with PBS-iECs/iCMs, SpGel and PBS (33.04 ± 7.13% vs 44.59 ± 3.80% and 60.40 ± 4.30%, respectively). The results also demonstrated a higher survival rate and integration of SpGel-encapsulated cells (iCMs, MLC2V, green) than cells alone in the infarcted hearts (Fig. 8A). As shown in Fig. 8B–E, the arterial and capillary densities in the SpGel-iEC/iCM-treated group were significantly higher than those in the PBS group, indicating that treatment with SpGel-iECs/iCMs promoted neovascularization in the infarcted region. Overall, we demonstrated improved cardiac function, reduced infarct size, increased capillary density, and improved cell graft retention in SpGel-iEC/iCM-treated MI mice.

Supplementary video related to this article can be found at https://doi.org/10.1016/j.bioactmat.2021.04.010

4. Discussion

In this study, we show that thermoresponsive nanofibrous SpGel could be used as an ideal platform for hiPSC attachment and differentiation, and it may serve as an injectable cell therapy carrier to enhance cell transplantation and promote cardiac repair. The tissue specificity of SpGel was investigated by proteomic analysis. A comparison was conducted between Sp-Gel and Myo-Gel, and the results showed that Sp-Gel shared 80% of the total protein species in Myo-Gel, including collagen I, collagen IV, fibronectin, laminin, elastin and growth factors, which is consistent with previous studies [29,34]. Sp-Gel may play an important role in cardiac repair, similar to Myo-Gel. Moreover, we found 623 other tissue-specific protein species in the Sp-Gel that were associated with biological process and molecular function terms. Proteins related to cell-substrate adhesion, gap junctions, cardiac muscle contraction, adrenergic signaling in CMs and the Wnt signaling pathway were highly expressed in Sp-Gel. Proteins related to cardiac regeneration and repair, such as agrin [35], TGF-β [36] and EGF [37], were also identified in Sp-Gel by MS analysis.

Since Wnt signaling promotes CM [2,38] and EC [39,40] differentiation from hPSCs, SpGel may serve as a platform for hiPSC differentiation into ECs and CMs. Previous studies have suggested that ECM and substrate stiffness affect the differentiation of MSCs into cells such as osteogenic cells, neural cells, and adipocytes via various signaling pathways, such as the ROCK, FAK, Src, ERK, and MAP kinase pathways [41–44]. hiPSCs were seeded on SpGel and were able to proliferate and express the pluripotency protein OCT4. Following the endothelial and

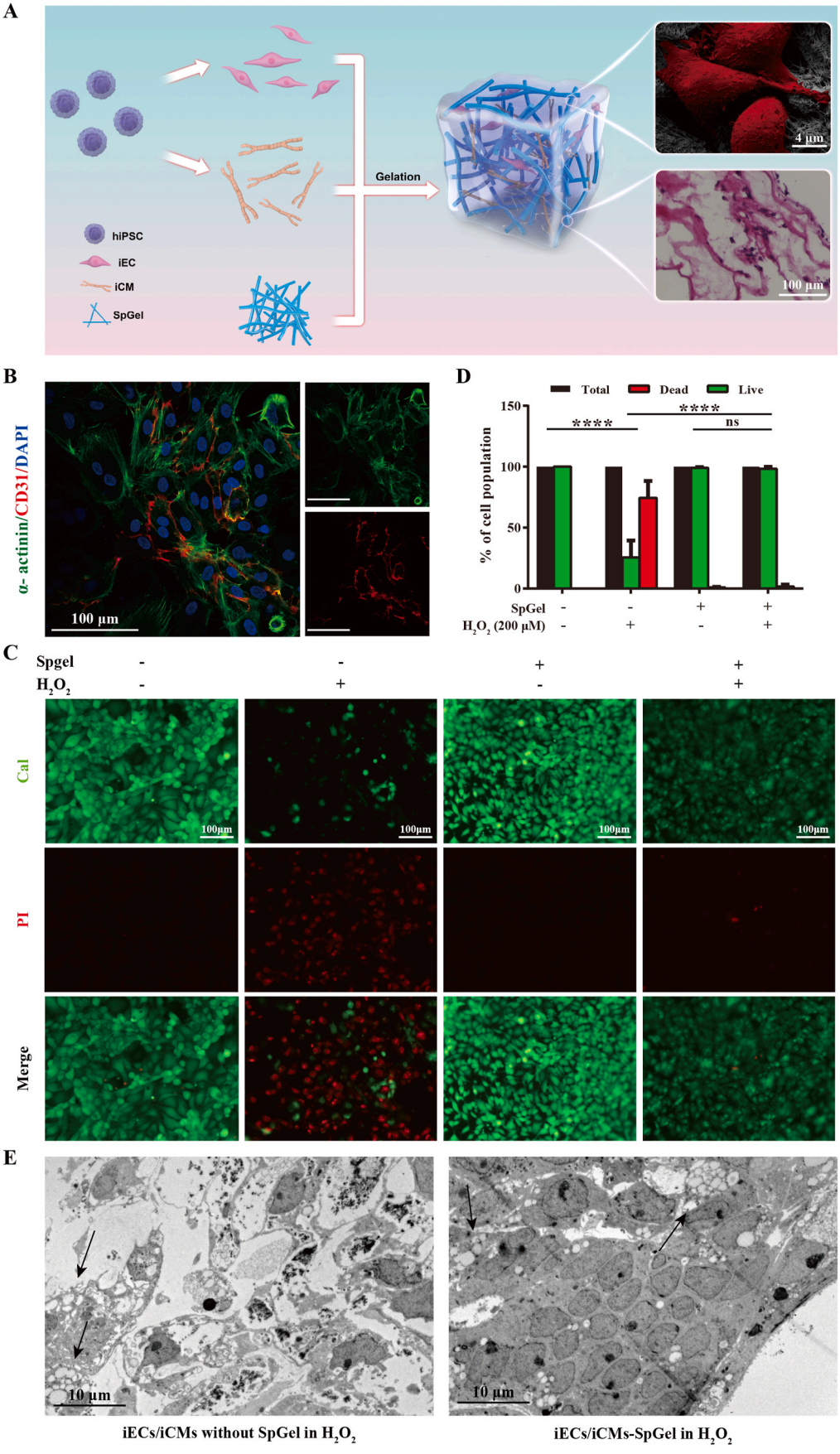

Fig. 5. Cytoprotective effects of SpGel encapsulation against H_2O_2. (A) Schematic of the three-dimensional culture model of iECs and iCMs in SpGel. (B) Immunostaining of cocultured iCMs (α-actinin, green) and iECs (CD31, red) and nuclei (blue). (C) Encapsulation of iECs/iCMs with SpGel increased cell survival in the presence of H_2O_2 (200 μM), as determined by the live/dead assay. (D) Quantitative analysis of cell survival levels (**** $p < 0.0001$). (E) Ultrastructural analysis of iECs/iCMs in H_2O_2 with or without SpGel. Arrows indicate apoptosis and cell vacuolation. (For interpretation of the references to color in this figure legend, the reader is referred to the Web version of this article.)

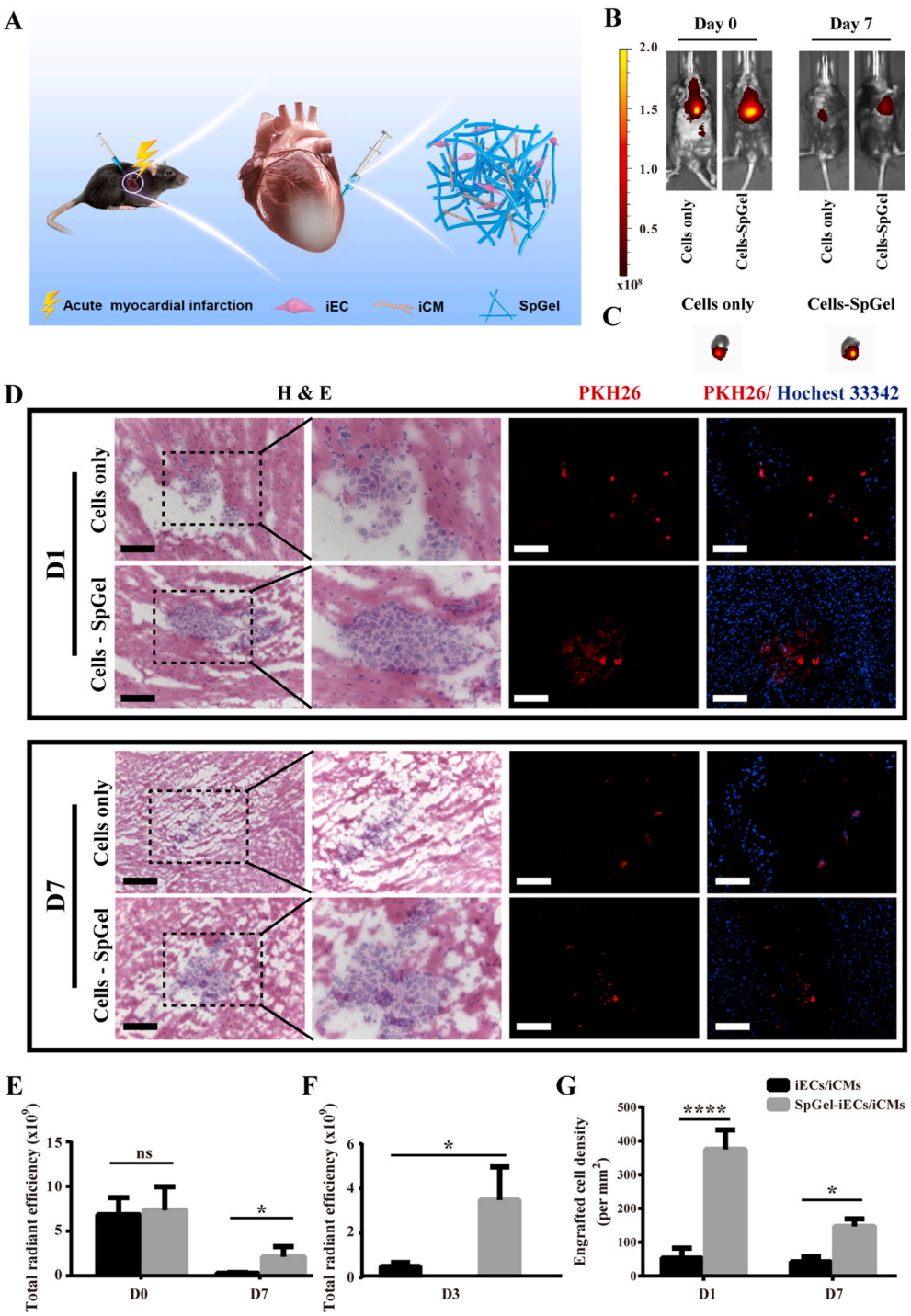

Fig. 6. Survival and engraftment of iECs/iCMs after injection into MI mouse hearts. (A) Schematic of animal experiments to explore the possible treatment of iECs/iCMs with SpGel in a mouse MI model. (B) DiR-labeled iECs/iCMs imaged under IVIS showing retention in each group on day 0 and day 7 post injection. (C) Fluorescence imaging of the heart on day 3 post injection. (D) Day 1 and day 7 after injection of PKH26-labeled (red) iECs/iCMs with or without SpGel. Representative H&E staining and immunostaining of sectioned heart tissues. Scale bars = 100 μm. Quantitative analysis of (E) *in vivo* IVIS epifluorescence measurements and (F) fluorescence imaging in the heart. (G) Quantitative analysis of engrafted cell density on days 1 and 7 (* $p < 0.05$, **** $p < 0.0001$). (For interpretation of the references to color in this figure legend, the reader is referred to the Web version of this article.)

cardiac differentiation protocol, hiPSCs efficiently differentiated into ECs and CMs, respectively. CM-specific and EC-specific markers were identified in the two kinds of induced cells. ECs induced on SpGel exhibited tube-forming ability similar to that of HUVECs. Interestingly, iCMs induced on SpGel showed a higher beating frequency and FP amplitude than those induced on Matrigel, suggesting that SpGel may promote the functional improvement of iCMs [45]. Since the safety of mouse sarcoma tumor-derived Matrigel for clinical applications remains to be evaluated [46], our work indicated that SpGel could replace Matrigel as a supporting microenvironment for iPSC culture and differentiation. Yiwei Xu et al. also reported that a spinal cord-derived DSCM gel could be used for 3D culture of neural stem/progenitor cells (NSPCs) and demonstrated that the DSCM gel promoted the proliferation, migration and differentiation of NSPCs [26]. An ECM hydrogel derived from human omental tissues also demonstrated efficient cardiac, cortical and adipogenic differentiation within the hydrogel [47].

From mass spectrometry data, the downregulated oxidation-reduction process, as well as upregulated cell-substrate adhesion and extracellular structure organization process in SpGel, suggested that SpGel could be used as a carrier for cell transplantation, which might yield greater benefits than commonly utilized myocardial ECM hydrogel alone in the treatment of myocardial infarction. Cell retention was significantly improved in SpGel-encapsulated cell grafts one week after MI. Intramyocardial injection of SpGel-loaded iECs/iCMs efficiently

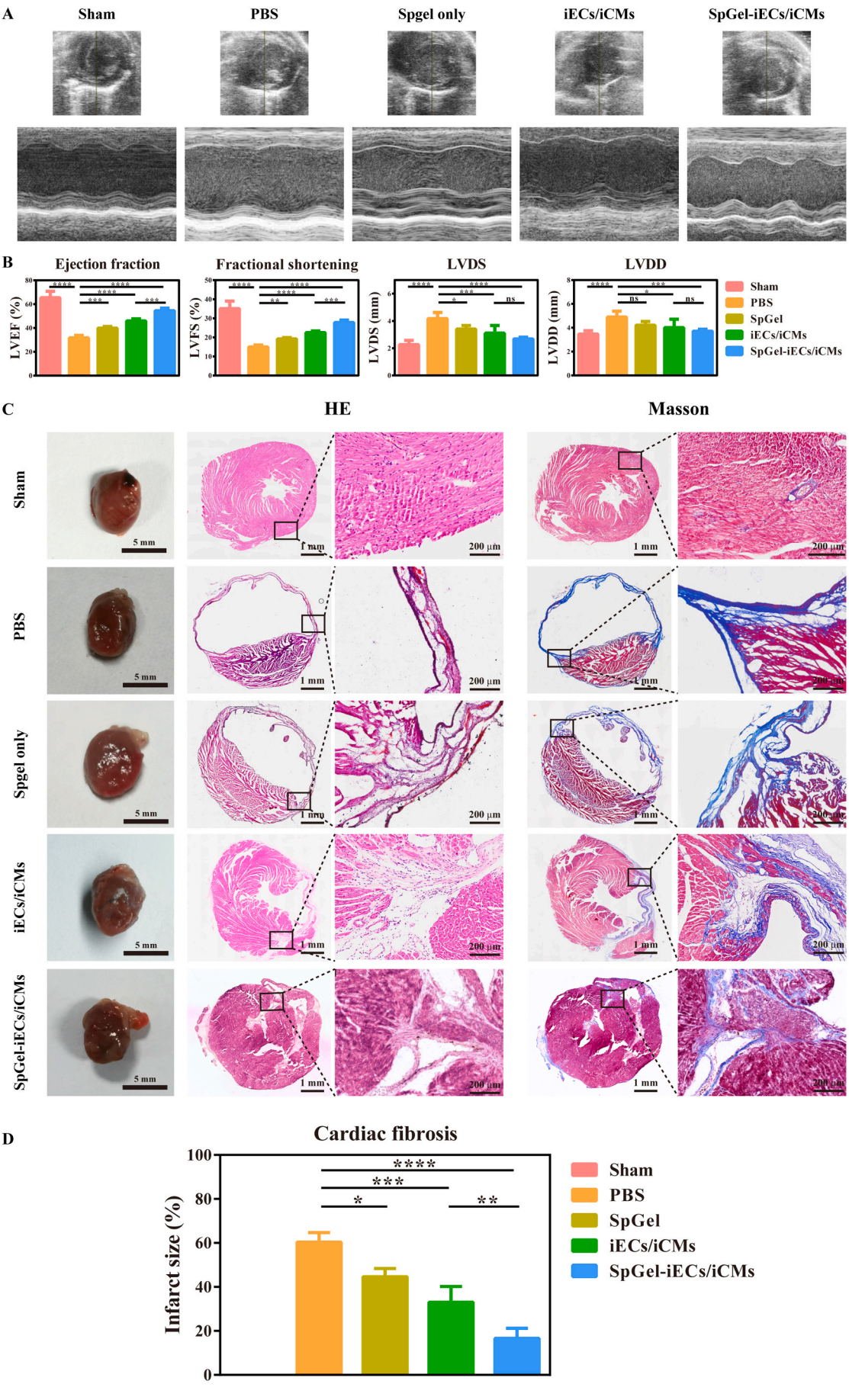

(caption on next page)

Fig. 7. Enhancement of cardiac function and reduction in cardiac fibrosis by SpGel-iEC/iCM injection after myocardial infarction. (A) Echocardiographic measurement of cardiac function of mice in different treatment groups on day 28 after myocardial infarction. (B) Statistical analysis of ejection fraction, fractional shortening, LVDS and LVDD was performed based on the echocardiographic results (n = 7, * $p < 0.05$, ** $p < 0.01$, *** $p < 0.001$, **** $p < 0.0001$). (C) Heart photography, H&E staining and Masson staining of mouse hearts in different treatment groups at day 28 after myocardial infarction. (D) Statistical analysis of the infarct size based on Masson's staining.

preserved the cardiac fraction and promoted neovascularization compared to the control PBS injection. SpGel may provide cell grafts with a microenvironment favorable for cell attachment and vascularization. We also observed that SpGel injection alone mildly increased the cardiac function and angiogenesis in the infarcted tissues, which may be related to the presence of structural matrix proteins, GAGs [48] and growth factors (including agrin [35], TGF-β [36] and EGF [37]) in SpGel. Since ECM degradation products have been reported to have mitogenic and chemoattractant effects on endothelial cells and stem cells [11,49], SpGel degradation products might play a role in cardiac function repair and neoangiogenesis.

Due to the high biocompatibility and 3D bioprinting property of SpGel, SpGel bioink combined with free-form printing technology would be one of the right candidates to print cell–laden structures and fabricate

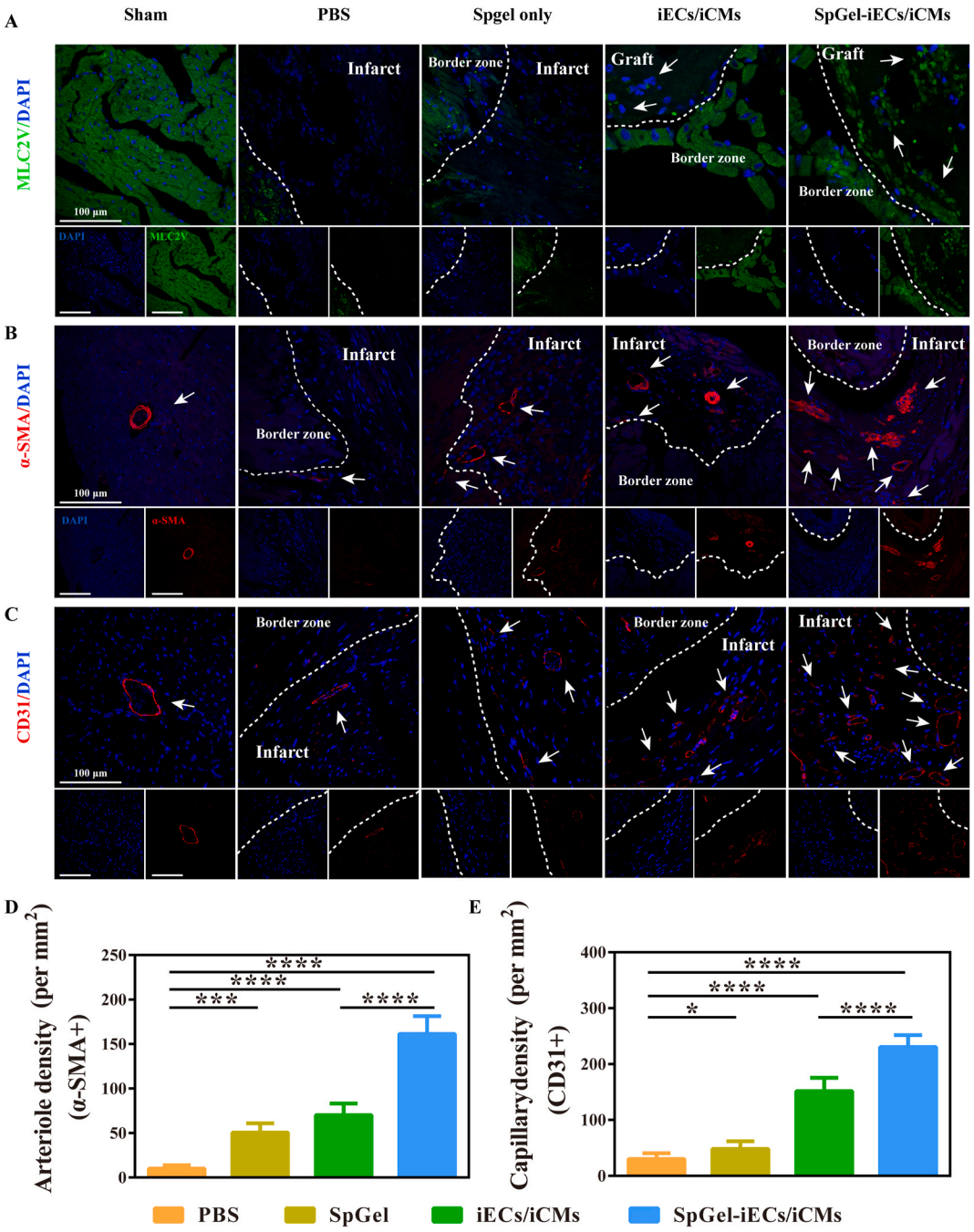

Fig. 8. The increase in cell graft retention and angiogenesis after SpGel-iEC/iCM injection. Immunofluorescence staining of (A) MLC2V (green), (B) α-SMA (red) (C) CD31 (red) at day 28 after myocardial infarction. Quantitative analysis of (D) arteriole density (α-SMA+) and (E) capillary density ($CD31^+$) (* $p < 0.05$, *** $p < 0.001$, **** $p < 0.0001$). (For interpretation of the references to color in this figure legend, the reader is referred to the Web version of this article.)

complex biological structures, which is a promising approach for organ and tissue engineering [17]. For the application of 3D printing SpGel patches, structural modification of enhanced bioadhesive and mechanical properties will be the object of future studies [50]. In further studies, the molecular mechanisms of functional improvement in cardiac differentiation and the antioxidant and cardiac repair mechanisms of SpGel need to be elucidated. Large animal models of myocardial ischemia will also be applied to validate the efficacy of treatment with SpGel-encapsulated iECs/iCMs for preclinical research.

5. Conclusion

In conclusion, we developed a thermoresponsive nanofibrous splenic matrix hydrogel (SpGel) to maintain the culture and promote the differentiation of hiPSCs. *In vivo* study indicated that application of SpGel-encapsulated iEC/iCMs effectively improved cell graft retention, accelerated cardiac function recovery, inhibited fibrosis and promoted revascularization of ischemic tissue. Moreover, SpGel could also be used as a biocompatible bioink for 3D printing cardiac organoids in the future. This study revealed that SpGel could be used as a platform for the culture and differentiation of hiPSCs, and an injectable cell transplantation carrier for regenerative medicine research and clinical utility.

CRediT authorship contribution statement

Ge Guan: Conceptualization, Methodology, Investigation, Writing - original draft, Writing - review & editing. **Da Huo:** Formal analysis, Software, Writing - review & editing. **Yanzhao Li:** Conceptualization, Writing - original draft, Writing - review & editing. **Xiaolin Zhao:** Methodology. **Yinghao Li:** Methodology, Investigation. **Zhongliang Qin:** Methodology, Investigation. **Dayu Sun:** Conceptualization, Methodology. **Guanyuan Yang:** Methodology. **Mingcan Yang:** Methodology, Investigation. **Ju Tan:** Methodology, Investigation. **Wen Zeng:** Funding acquisition, Methodology, Investigation. **Chuhong Zhu:** Funding acquisition, Conceptualization, Supervision, Writing - review & editing.

Declaration of competing interest

The authors declare that they have no known competing financial interests or personal relationships that could have appeared to influence the work reported in this paper.

Acknowledgements

This work was supported by the Key projects of the National Natural Science Foundation of China (No. 81830055), National Science Fund for Distinguished Young Scholars (No. 31625011), the National Key Research and Development Program (No. 2016YFC1101100), the National Science Fund for Outstanding Young Scholars (No. 31822021).

Appendix A. Supplementary data

Supplementary data to this article can be found online at https://doi.org/10.1016/j.bioactmat.2021.04.010.

References

[1] G. Burden, G.A. Roth, G.A. Mensah, C.O. Johnson, G. Addolorato, E. Ammirati, L. M. Baddour, M. Banach, N.C. Barengo, A.Z. Beaton, E.J. Benjamin, C.P. Benziger, A. Bonny, M. Brauer, M. Brodmann, T.J. Cahill, J. Carapetis, A.L. Catapano, S. S. Chugh, L.T. Cooper, J. Coresh, M. Criqui, N. DeCleene, K.A. Eagle, S. Emmons-Bell, V.L. Feigin, J. Fernández-Solà, G. Fowkes, E. Gakidou, S.M. Grundy, F.J. He, G. Howard, F. Hu, J.J. Jóźwiak, aa Lesley Inker, bb Ganesan Karthikeyan, cc Nicholas Kassebaum, W. Koroshetz, dd Carl Lavie, ee Donald Lloyd-Jones, ff S. Hong Lu, gg Antonio Mirijello, hh Awoke Misganaw Temesgen, A. Mokdad, A. E. Moran, ii Paul Muntner, J. Narula, jj Bruce Neal, kk Mpiko Ntsekhe, ll Glaucia Moraes de Oliveira, mm Catherine Otto, M. Owolabi, nn Michael Pratt, S. Rajagopalan, oo Marissa Reitsma, pp P. Antonio Luiz Ribeiro, qq Nancy Rigotti, rr Anthony Rodgers, tt Craig Sable, uu Saate Shakil, K. Sliwa-Hahnle, ll Benjamin Stark, J. Sundström, vv Patrick Timpel, ww M. Imad Tleyjeh, xx Marco Valgimigli, yy Theo Vos, P.K. Whelton, zz Magdi Yacoub, tt Liesl Zuhlke, ll Christopher Murray, V. Fuster, G. Rotondo, Global burden of cardiovascular diseases and risk factors, 1990–2019: update from the GBD 2019 study, J. Am. Coll. Cardiol. 76 (2020), https://doi.org/10.1016/j.jacc.2020.11.010.

[2] Y.W. Liu, B. Chen, X. Yang, J.A. Fugate, F.A. Kalucki, A. Futakuchi-Tsuchida, L. Couture, K.W. Vogel, C.A. Astley, A. Baldessari, J. Ogle, C.W. Don, Z. L. Steinberg, S.P. Seslar, S.A. Tuck, H. Tsuchida, A.V. Naumova, S.K. Dupras, M. S. Lyu, J. Lee, D.W. Hailey, H. Reinecke, L. Pabon, B.H. Fryer, W.R. MacLellan, R. S. Thies, C.E. Murry, Human embryonic stem cell-derived cardiomyocytes restore function in infarcted hearts of non-human primates, Nat. Biotechnol. 36 (2018) 597–605, https://doi.org/10.1038/nbt.4162.

[3] J. Zhang, L.F. Chu, Z. Hou, M.P. Schwartz, T. Hacker, V. Vickerman, S. Swanson, N. Leng, B.K. Nguyen, A. Elwell, J. Bolin, M.E. Brown, R. Stewart, W.J. Burlingham, W.L. Murphy, J.A. Thomson, Functional characterization of human pluripotent stem cell-derived arterial endothelial cells, Proc. Natl. Acad. Sci. U.S.A. 114 (2017) E6072–E6078, https://doi.org/10.1073/pnas.1702295114.

[4] Y. Jiang, X.L. Lian, Heart regeneration with human pluripotent stem cells: prospects and challenges, Bioact. Mater. 5 (2020) 74–81, https://doi.org/10.1016/j.bioactmat.2020.01.003.

[5] S.J. Lee, Y.D. Sohn, A. Andukuri, S. Kim, J. Byun, J.W. Han, I.H. Park, H.W. Jun, Y. S. Yoon, Enhanced therapeutic and long-term dynamic vascularization effects of human pluripotent stem cell-derived endothelial cells encapsulated in a nanomatrix gel, Circulation 136 (2017) 1939–1954, https://doi.org/10.1161/CIRCULATIONAHA.116.026329.

[6] U. Goyal, M. Ta, A novel role of vitronectin in promoting survival of mesenchymal stem cells under serum deprivation stress, Stem Cell Res. Ther. (2020), https://doi.org/10.1186/s13287-020-01682-y.

[7] E. Tous, B. Purcell, J.L. Ifkovits, J.A. Burdick, Injectable acellular hydrogels for cardiac repair, J. Cardiovasc. Transl. Res. (2011), https://doi.org/10.1007/s12265-011-9291-1.

[8] K. Zhang, Z. Jia, B. Yang, Q. Feng, X. Xu, W. Yuan, X. Li, X. Chen, L. Duan, D. Wang, L. Bian, Adaptable hydrogels mediate cofactor-assisted activation of biomarker-responsive drug delivery via positive feedback for enhanced tissue regeneration, Adv. Sci. 5 (2018), https://doi.org/10.1002/advs.201800875.

[9] Q. Feng, J. Xu, K. Zhang, H. Yao, N. Zheng, L. Zheng, J. Wang, K. Wei, X. Xiao, L. Qin, L. Bian, Dynamic and cell-infiltratable hydrogels as injectable carrier of therapeutic cells and drugs for treating challenging bone defects, ACS Cent. Sci. (2019), https://doi.org/10.1021/acscentsci.8b00764.

[10] W.C.W. Chen, Z. Wang, M.A. Missinato, D.W. Park, D.W. Long, H.J. Liu, X. Zeng, N. A. Yates, K. Kim, Y. Wang, Decellularized zebrafish cardiac extracellular matrix induces mammalian heart regeneration, Sci. Adv. (2016), https://doi.org/10.1126/sciadv.1600844.

[11] K.H. Hussein, K.M. Park, L. Yu, H.H. Kwak, H.M. Woo, Decellularized hepatic extracellular matrix hydrogel attenuates hepatic stellate cell activation and liver fibrosis, Mater. Sci. Eng. C 116 (2020) 111160, https://doi.org/10.1016/j.msec.2020.111160.

[12] N. Rao, G. Agmon, M.T. Tierney, J.L. Ungerleider, R.L. Braden, A. Sacco, K. L. Christman, Engineering an injectable muscle-specific microenvironment for improved cell delivery using a nanofibrous extracellular matrix hydrogel, ACS Nano 11 (2017) 3851–3859, https://doi.org/10.1021/acsnano.7b00093.

[13] J.M. Vieira, S. Norman, C.V. Del Campo, T.J. Cahill, D.N. Barnette, M. Gunadasa-Rohling, L.A. Johnson, D.R. Greaves, C.A. Carr, D.G. Jackson, P.R. Riley, The cardiac lymphatic system stimulates resolution of inflammation following myocardial infarction, J. Clin. Invest. (2018), https://doi.org/10.1172/JCI97192.

[14] M.R. Harrison, X. Feng, G. Mo, A. Aguayo, J. Villafuerte, T. Yoshida, C.A. Pearson, S. Schulte-Merker, L. Ching-Ling, Late developing cardiac lymphatic vasculature supports adult zebrafish heart function and regeneration, Elife (2019), https://doi.org/10.7554/eLife.42762.

[15] X. Liu, E. De la Cruz, X. Gu, L. Balint, M. Oxendine-Burns, T. Terrones, W. Ma, H. H. Kuo, C. Lantz, T. Bansal, E. Thorp, P. Burridge, Z. Jakus, J. Herz, O. Cleaver, M. Torres, G. Oliver, Lymphoangiocrine signals promote cardiac growth and repair, Nature (2020), https://doi.org/10.1038/s41586-020-2998-x.

[16] H.R. Lieder, P. Kleinbongard, A. Skyschally, H. Hagelschuer, W.M. Chilian, G. Heusch, Vago-splenic axis in signal transduction of remote ischemic preconditioning in pigs and rats, Circ. Res. (2018), https://doi.org/10.1161/CIRCRESAHA.118.313859.

[17] G. Heusch, The spleen in myocardial infarction, Circ. Res. 124 (2019) 26–28, https://doi.org/10.1161/CIRCRESAHA.118.314331.

[18] J. Xiang, X. Zheng, P. Liu, L. Yang, D. Dong, W. Wu, X. Liu, J. Li, Y. Lv, Decellularized spleen matrix for reengineering functional hepatic-like tissue based on bone marrow mesenchymal stem cells, Organogenesis 12 (2016) 128–142. https://nam03.safelinks.protection.outlook.com/?url=https%3A%2F%2Fdoi.org%2F10.1080%2F15476278.2016.1185584&data=04%7C01%7Cj.dhakshnamoorthy%40elsevier.com%7Cdcf7994790d04556f88908d90bec4479%7C9274ee3f94254109a27f9fb15c10675d%7C0%7C0%7C637553931677973406%7CUnknown%7CTWFpbGZsb3d8eyJWIjoiMC4wLjAwMDAiLCJQIjoiV2luMzIiLCJBTiI6Ik1haWwiLCJXVCI6Mn0%3D%7C3000&sdata=LGoqiOL38TpwAivITcvkHOIPMbJk0wX1jjHx68Y2Th4%3D&reserved=0.

[19] Z. Lokmic, T. Lämmermann, M. Sixt, S. Cardell, R. Hallmann, L. Sorokin, The extracellular matrix of the spleen as a potential organizer of immune cell compartments, Semin. Immunol. 20 (2008) 4–13, https://doi.org/10.1016/j.smim.2007.12.009.

[20] R. Gao, W. Wu, J. Xiang, Y. Lv, X. Zheng, Q. Chen, H. Wang, B. Wang, Z. Liu, F. Ma, Hepatocyte culture in autologous decellularized spleen matrix, Organogenesis 11 (2015) 16–29, https://doi.org/10.1080/15476278.2015.1011908.
[21] M. Mito, H. Ebata, M. Kusano, T. Onishi, T. Saito, S. Sakamoto, Morphology and function of isolated hepatocytes transplanted into rat spleen, Transplantation (1979), https://doi.org/10.1097/00007890-197912000-00013.
[22] G.M. Crane, E. Jeffery, S.J. Morrison, Adult haematopoietic stem cell niches, Nat. Rev. Immunol. 17 (2017) 573–590, https://doi.org/10.1038/nri.2017.53.
[23] J.M. Singelyn, P. Sundaramurthy, T.D. Johnson, P.J. Schup-Magoffin, D.P. Hu, D. M. Faulk, J. Wang, K.M. Mayle, K. Bartels, M. Salvatore, A.M. Kinsey, A. N. Demaria, N. Dib, K.L. Christman, Catheter-deliverable hydrogel derived from decellularized ventricular extracellular matrix increases endogenous cardiomyocytes and preserves cardiac function post-myocardial infarction, J. Am. Coll. Cardiol. 59 (2012) 751–763, https://doi.org/10.1016/j.jacc.2011.10.888.
[24] M.P. Francis, E. Breathwaite, A.A. Bulysheva, F. Varghese, R.U. Rodriguez, S. Dutta, I. Semenov, R. Ogle, A. Huber, A.M. Tichy, S. Chen, C. Zemlin, Human placenta hydrogel reduces scarring in a rat model of cardiac ischemia and enhances cardiomyocyte and stem cell cultures, Acta Biomater. 52 (2017) 92–104, https://doi.org/10.1016/j.actbio.2016.12.027.
[25] G.G. Giobbe, C. Crowley, C. Luni, S. Campinoti, M. Khedr, K. Kretzschmar, M.M. De Santis, E. Zambaiti, F. Michielin, L. Meran, Q. Hu, G. van Son, L. Urbani, A. Manfredi, M. Giomo, S. Eaton, D. Cacchiarelli, V.S.W. Li, H. Clevers, P. Bonfanti, N. Elvassore, P. De Coppi, Extracellular matrix hydrogel derived from decellularized tissues enables endodermal organoid culture, Nat. Commun. 10 (2019), https://doi.org/10.1038/s41467-019-13605-4.
[26] Y. Xu, J. Zhou, C. Liu, S. Zhang, F. Gao, W. Guo, X. Sun, C. Zhang, H. Li, Z. Rao, S. Qiu, Q. Zhu, X. Liu, X. Guo, Z. Shao, Y. Bai, X. Zhang, D. Quan, Understanding the role of tissue-specific decellularized spinal cord matrix hydrogel for neural stem/progenitor cell microenvironment reconstruction and spinal cord injury, Biomaterials 268 (2021) 120596, https://doi.org/10.1016/j.biomaterials.2020.120596.
[27] M. Li, A. Zhang, J. Li, J. Zhou, Y. Zheng, C. Zhang, D. Xia, H. Mao, J. Zhao, Osteoblast/fibroblast coculture derived bioactive ECM with unique matrisome profile facilitates bone regeneration, Bioact. Mater. 5 (2020) 938–948, https://doi.org/10.1016/j.bioactmat.2020.06.017.
[28] N. Noor, A. Shapira, R. Edri, I. Gal, L. Wertheim, T. Dvir, 3D printing of personalized thick and perfusable cardiac patches and hearts, Adv. Sci. 6 (2019) 1900344, https://doi.org/10.1002/advs.201900344.
[29] T. Deuse, X. Hu, A. Gravina, D. Wang, G. Tediashvili, C. De, W.O. Thayer, A. Wahl, J.V. Garcia, H. Reichenspurner, M.M. Davis, L.L. Lanier, S. Schrepfer, Hypoimmunogenic derivatives of induced pluripotent stem cells evade immune rejection in fully immunocompetent allogeneic recipients, Nat. Biotechnol. 37 (2019) 252–258, https://doi.org/10.1038/s41587-019-0016-3.
[30] P.W. Burridge, E. Matsa, P. Shukla, Z.C. Lin, J.M. Churko, A.D. Ebert, F. Lan, S. Diecke, B. Huber, N.M. Mordwinkin, J.R. Plews, O.J. Abilez, B. Cui, J.D. Gold, J. C. Wu, Chemically defned generation of human cardiomyocytes, Nat. Methods 11 (2014) 855–860, https://doi.org/10.1038/nMeth.2999.
[31] D. Jhala, H. Rather, D. Kedaria, J. Shah, S. Singh, R. Vasita, Biomimetic polycaprolactone-chitosan nanofibrous substrate influenced cell cycle and ECM secretion affect cellular uptake of nanoclusters, Bioact. Mater. 4 (2019) 79–86, https://doi.org/10.1016/j.bioactmat.2018.12.004.
[32] O. Chaudhuri, J. Cooper-White, P.A. Janmey, D.J. Mooney, V.B. Shenoy, Effects of extracellular matrix viscoelasticity on cellular behaviour, Nature 584 (2020) 535–546, https://doi.org/10.1038/s41586-020-2612-2.
[33] J. Ding, Y. Yao, J. Li, Y. Duan, J.R. Nakkala, X. Feng, W. Cao, Y. Wang, L. Hong, L. Shen, Z. Mao, Y. Zhu, C. Gao, A reactive oxygen species scavenging and O2 generating injectable hydrogel for myocardial infarction treatment in vivo, Small 2005038 (2020) 1–9, https://doi.org/10.1002/smll.202005038.
[34] N.G. Frangogiannis, The extracellular matrix in myocardial injury, repair, and remodeling, J. Clin. Invest. 127 (2017) 1600–1612, https://doi.org/10.1172/JCI87491.
[35] E. Bassat, Y.E. Mutlak, A. Genzelinakh, I.Y. Shadrin, K.B. Umansky, O. Yifa, D. Kain, D. Rajchman, J. Leach, D.R. Bassat, Y. Udi, R. Sarig, I. Sagi, J.F. Martin, N. Bursac, The extracellular matrix protein agrin promotes heart regeneration in mice, Nat. Publ. Gr. 547 (2017) 179–184, https://doi.org/10.1038/nature22978.
[36] F. Chablais, A. Jaźwińska, The regenerative capacity of the zebrafish heart is dependent on TGFβ signaling, Development (2012), https://doi.org/10.1242/dev.078543.
[37] M.E. Reichelt, S. O'Brien, W.G. Thomas, J.P. Headrick, Transactivation of the epidermal growth factor receptor in responses to myocardial stress and cardioprotection, Int. J. Biochem. Cell Biol. (2017), https://doi.org/10.1016/j.biocel.2016.12.014.
[38] V.C. Chen, J. Ye, P. Shukla, G. Hua, D. Chen, Z. Lin, J. chang Liu, J. Chai, J. Gold, J. Wu, D. Hsu, L.A. Couture, Development of a scalable suspension culture for cardiac differentiation from human pluripotent stem cells, Stem Cell Res. (2015), https://doi.org/10.1016/j.scr.2015.08.002.
[39] P.S. Woll, J.K. Morris, M.S. Painschab, R.K. Marcus, A.D. Kohn, T.L. Biechele, R. T. Moon, D.S. Kaufman, Wnt signaling promotes hematoendothelial cell development from human embryonic stem cells, Blood (2008), https://doi.org/10.1182/blood-2007-04-084186.
[40] X. Lian, X. Bao, A. Al-Ahmad, J. Liu, Y. Wu, W. Dong, K.K. Dunn, E.V. Shusta, S. P. Palecek, Efficient differentiation of human pluripotent stem cells to endothelial progenitors via small-molecule activation of WNT signaling, Stem Cell Rep. (2014), https://doi.org/10.1016/j.stemcr.2014.09.005.
[41] E.K.F. Yim, E.M. Darling, K. Kulangara, F. Guilak, K.W. Leong, Nanotopography-induced changes in focal adhesions, cytoskeletal organization, and mechanical properties of human mesenchymal stem cells, Biomaterials (2010), https://doi.org/10.1016/j.biomaterials.2009.10.037.
[42] J. Du, X. Chen, X. Liang, G. Zhang, J. Xu, L. He, Q. Zhan, X.Q. Feng, S. Chien, C. Yang, Integrin activation and internalization on soft ECM as a mechanism of induction of stem cell differentiation by ECM elasticity, Proc. Natl. Acad. Sci. U.S. A. (2011), https://doi.org/10.1073/pnas.1106467108.
[43] Y.R.V. Shih, K.F. Tseng, H.Y. Lai, C.H. Lin, O.K. Lee, Matrix stiffness regulation of integrin-mediated mechanotransduction during osteogenic differentiation of human mesenchymal stem cells, J. Bone Miner. Res. (2011), https://doi.org/10.1002/jbmr.278.
[44] J.E. Dixon, D.A. Shah, C. Rogers, S. Hall, N. Weston, C.D.J. Parmenter, D. McNally, C. Denning, K.M. Shakesheff, Combined hydrogels that switch human pluripotent stem cells from self-renewal to differentiation, Proc. Natl. Acad. Sci. U.S.A. (2014), https://doi.org/10.1073/pnas.1319685111.
[45] M.O. Lee, K.B. Jung, S.J. Jo, S.A. Hyun, K.S. Moon, J.W. Seo, S.H. Kim, M.Y. Son, Modelling cardiac fibrosis using three-dimensional cardiac microtissues derived from human embryonic stem cells, J. Biol. Eng. 13 (2019) 1–17, https://doi.org/10.1186/s13036-019-0139-6.
[46] F. Mannello, G.A. Tonti, Concise review: no breakthroughs for human mesenchymal and embryonic stem cell culture: conditioned medium, feeder layer, or feeder-free; medium with fetal calf serum, human serum, or enriched plasma; serum-free, serum replacement nonconditioned medium, or Ad Hoc formula? All That Glitters Is Not Gold!, Stem Cells 25 (2007) 1603–1609, https://doi.org/10.1634/stemcells.2007-0127.
[47] R. Edri, I. Gal, N. Noor, T. Harel, S. Fleischer, N. Adadi, O. Green, D. Shabat, L. Heller, A. Shapira, I. Gat-Viks, D. Peer, T. Dvir, Personalized hydrogels for engineering diverse fully autologous tissue implants, Adv. Mater. 31 (2019) 1–9, https://doi.org/10.1002/adma.201803895.
[48] R.R. Costa, D. Soares da Costa, R.L. Reis, I. Pashkuleva, Bioinspired baroplastic glycosaminoglycan sealants for soft tissues, Acta Biomater. 87 (2019) 108–117, https://doi.org/10.1016/j.actbio.2019.01.040.
[49] A.J. Beattie, T.W. Gilbert, J.P. Guyot, A.J. Yates, S.F. Badylak, Chemoattraction of progenitor cells by remodeling extracellular matrix scaffolds, Tissue Eng. (2009), https://doi.org/10.1089/ten.tea.2008.0162.
[50] X. Xu, X. Xia, K. Zhang, A. Rai, Z. Li, P. Zhao, K. Wei, L. Zou, B. Yang, W.K. Wong, P.W.Y. Chiu, L. Bian, Bioadhesive hydrogels demonstrating pH-independent and ultrafast gelation promote gastric ulcer healing in pigs, Sci. Transl. Med. 12 (2020), https://doi.org/10.1126/SCITRANSLMED.ABA8014.